Journal of Engineering and Sustainable Development
Vol. 30, No. 05, August 2026
https://jeasd.uomustansiriyah.edu.iq/index.php/jeasd
ISSN 2520-0917
Research Article
https://doi.org/10.31272/jeasd.3917

Multi-Objective Optimized Machine Learning for Early Fault Detection in Water-Cooled Chillers

Nguyen Duc Thanh, Dinh Anh Tuan Tran *

Faculty of Heat and Refrigeration Engineering, Industrial University of Ho Chi Minh City, Ho Chi Minh City, Viet Nam

*Email: trandinhanhtuan@iuh.edu.vn

Article Info

Received 04/02/2026

Revised 18/07/2026

Accepted 06/08/2026

Abstract

In large office buildings and commercial complexes, HVAC systems account for nearly two-thirds of total electricity consumption. However, early fault detection and diagnosis (FDD) in water-cooled chillers remains challenging because faults usually develop slowly, produce weak initial signatures, and exhibit strongly nonlinear thermodynamic behavior. Moreover, overlapping operational characteristics between faults make accurate diagnosis under mild and moderate conditions difficult. Previous studies using the ASHRAE RP-1043 dataset reported limited diagnostic performance for incipient faults, particularly refrigerant leakage and condenser fouling. To address these gaps, this study proposes a hybrid optimization-based FDD framework for early fault diagnosis in water-cooled chillers, integrating the Non-Dominated Sorting Genetic Algorithm III with Local Search (NSGA-III-LS) and the M5 Prime regression model for hyperparameter tuning and nonlinear operational modeling. The proposed framework offers a balanced trade-off between fault sensitivity, residual stability, and diagnostic accuracy. Validation results demonstrate high detection rates of 62.5-95.83% for mild faults and nearly 100% for severe faults, outperforming conventional methods, especially during incipient fault stages. The proposed method also supports earlier detection of abnormal thermal behavior, contributing to energy savings of approximately 15-30%, extended equipment lifespan, and more effective predictive maintenance planning.

Keywords: EWMA Control Chart, Fault Detection and Diagnosis, M5P Model Tree, Multi-Objective Optimization, NSGA-III.

1. Introduction

In large urban areas, the rapid growth if high-rise buildings and commercial centers have increased electricity demand during building operation. Heating, Ventilation, and Air Conditioning (HVAC) systems typically account for 40-60% of a building's total electricity consumption [1]. HVAC systems operate continuously and involve complex, nonlinear thermodynamic processes. Their performance is strongly affected by weather conditions, cooling load, and occupant behavior [2], [3]. Consequently, HVAC equipment is prone to performance degradation and operational faults over time.

In practice, many central air-conditioning systems, including water-cooled chillers, Air Handling Units (AHUs), and Variable Refrigerant Volume/Variable Refrigerant Flow (VRV/VRF) systems, are still operated and maintained using approaches such as Proportional-Integral-Derivative (PID) control or scheduled maintenance [4]. These strategies rely primarily on physical principles and operator expertise, with limited predictive maintenance capability. Therefore, signs of abnormal operation are often detected only after a serious incident has occurred [5]. Gradual performance degradation or undetected faults will reduce system reliability and increase energy consumption, maintenance costs, and equipment wear [6]. For these reasons, research on predictive maintenance is increasingly emphasized. In particular, fault detection and diagnosis (FDD) play a crucial role in monitoring and maintaining effective system operation. FDD strategies enhance reliability, improve energy efficiency, and support effective predictive maintenance planning.

Recently, advances in sensor technology and data acquisition have made it easier for mathematical models to fully exploit these advantages [7]. Data-driven methods such as machine learning (ML), deep learning (DL), Artificial Neural Networks (ANN), and Artificial Intelligence (AI) are increasingly applied in many fields, especially in water-cooled chiller systems for fault detection and diagnosis. This is because they can describe non-linear relationships between operational variables [8]. Algorithms such as Support Vector Regression (SVR), Random

Forest (RF), Gradient Boosting, Kriging, and decision tree-based regression models have been explored to determine the anomalous thermodynamic behavior in such systems [9], [10].

Among them, the M5 Prime (M5P) regression model combines decision tree partitioning with a linear regression model at the leaf nodes [11]. This structure not only enables the model to capture nonlinear system behavior but also maintains the interpretability of complex relationships [12]. Thanks to these advantages, M5P has been applied in many energy engineering, hydrological forecasting, traffic prediction, and industrial engineering studies [13], [14]. However, in the HVAC field, particularly in centrifugal water-cooled chiller systems, its application remains relatively limited. Although fault detection and diagnosis (FDD) methods have been applied, they still fall short of accuracy and reliability requirements. Therefore, substantial improvement in benchmark model performance is needed, requiring a systematic and well-structured optimization strategy.

Although machine learning models offer a certain degree of efficiency, their performance is still highly dependent on the proper selection of parameter settings and threshold values [15]. Therefore, over the past decade, significant progress has been made in metaheuristic optimization for parameter tuning in complex systems. Among these, Genetic Algorithms (GA), Particle Swarm Optimization (PSO), Differential Evolution (DE), and Ant Colony Optimization (ACO) have been widely adopted for the calibration of machine learning models across various applications [16], [17].

For example, Srivastava et al. [18] proposed an elitist genetic algorithm (EGA) combined with a random forest-based feature selection method to identify optimal input variables for short-term load forecasting using an M5P regression tree model. In the HVAC field, similar hybrid strategies have also been widely adopted. Xia et al. [19] integrated kernel Principal Component Analysis (KPCA) with a gravitational search algorithm (GSA)-optimized Least Squares Support Vector Machine (LSSVM) for multiclass fault classification in centrifugal chillers, while Liu et al. [20] developed an MSPSO-optimized XGBoost model, where XGBoost was also used for feature importance-based dimensionality reduction. Furthermore, the ASHRAE RP-1043 dataset is a widely used benchmark for chiller fault diagnosis, covering normal operating conditions, multiple fault types, and various operating scenarios, while the study by Li et al. [21] developed GA-optimized LightGBM frameworks to address imbalanced data conditions, achieving accuracy improvements of approximately 1.16% to 3.36% over benchmark methods [21]. Using NSGA-III to optimize machine learning models significantly boosts fault diagnosis accuracy without compromising multi-objective optimization performance [22]. Furthermore, in diverse scenarios, the prNSGA-III approach successfully cut environmental impact by up to 73% while boosting thermal comfort by 46% [23].

Extensive literature demonstrates the benefits of combining machine learning with optimization techniques for HVAC fault diagnosis and predictive maintenance [24]. However, most studies still focus on traditional modeling methods such as XGBoost, LightGBM, SVM, RF, and LSSVR. Studies on multi-objective optimization remain relatively limited. Few studies on water-cooled chiller systems simultaneously consider diagnostic accuracy, residual stability, and fault sensitivity under nonlinear and unbalanced conditions. Most methods rely on single-objective tuning or empirical parameter selection, which limits their applicability in practice. Early fault detection also remains a significant challenge. Faults such as refrigerant leakage and condenser fouling usually develop gradually. These faults exhibit low magnitude, high nonlinearity, and high sensitivity to noise. Consequently, fault detection at low severities remains unsatisfactory, though these incipient faults significantly degrade energy efficiency and system reliability. In contrast, NSGA-III is a robust, flexible framework for multi-objective optimization, owing to its adaptability in hybrid models [25]. Its Pareto-based mechanism further enables effective handling of complex problems with multiple conflicting objectives [26].

However, the application of the M5P model in centrifugal chiller fault diagnosis is still limited. To fix these issues, this paper integrates a Local Search mechanism into NSGA-III to target early-stage fault detection in water-cooled chillers. The contributions of this method, from both methodological and practical standpoints, are outlined below:

(i) Proposed the application of the NSGA-III optimization algorithm with local search to enhance convergence capability and solution quality in multi-objective machine learning problems.

(ii) Establish an experimental setting in MATLAB for multi-objective optimization to fine-tune the M5P model, allowing for systematic optimization of model parameters, integration with the Exponentially Weighted Moving Average (EWMA) control chart for early error detection and diagnosis, and maintaining a low false alarm.

(iii) Develop a comprehensive hybrid FDD approach (NSGA-III-LS-M5P) to ensure a balance between small-error detection sensitivity and prediction accuracy.

(iv) Develop a highly interpretive model capable of early detection of various critical faults such as refrigerant leakage and condenser fouling, thereby supporting appropriate predictive maintenance, minimizing operating costs, reducing energy consumption, and improving reliability in centrifugal water-cooled chiller systems.

Two difficult-to-identify fault types, refrigerant leakage and condenser fouling, were selected based on operational and performance characteristics from the benchmark dataset of the ASHRAE RP-1043 project. This was done to ensure an objective and fair comparison with previously published research. In addition, an EWMA control chart with a 99.73% confidence interval (corresponding to 3σ) was established.

2. Methodology

2.1. M5P-Based Model

The M5P (M5') model was developed by Wang and Witten (1997), with the addition of pruning and smoothing techniques to improve prediction efficiency [27], [28]. When implemented in MATLAB software, the M5P model has several practical advantages over other traditional models due to its simplification in terms of parameter adjustment, reduced training time, and stable convergence compared to methods such as ANN or SVM. The branched tree structure allows for fast computation and easy adaptation when integrated with residual-based methods such as EWMA plots in the FDD problem. In addition, the high interpretability of the M5P model elucidates physical mechanisms, which is especially important in systems with nonlinear disturbances in HVAC systems. These outstanding advantages make M5P a suitable choice for iterative and experimental optimization problems.

Selecting a training dataset $G = \{(x_i, y_i)\}_{i=1}^{m}$, the M5P model performs a local homogeneous recursive partitioning process based on decision rules. At each node, the relationships between input and output variables are approximated by a multivariate linear regression model, expressed by (1):

$$\hat{y} = \beta_0 + \sum_{j=1}^{p} \beta_i x_j + \epsilon \quad (1)$$

Equation (1) is defined as follows: $\hat{y}$ is the output value of the predictive model, x_j is the input variable corresponding to the main operating variable of the system, β_i denotes the regression coefficients estimated from the training data, p is the number of input variables, and ϵ is the residual error term.

The M5P model tree is constructed based on the Standard Deviation Reduction (SDR) criterion, a measure of variance used to evaluate each potential split. More precisely, the split algorithm maximizes SDR, aiming to minimize prediction errors on the resulting subsets. The SDR is defined in (2):

$$SDR = sd(T) - \sum_i \frac{|T_i|}{|T|}\, sd(T_i) \quad (2)$$

Where the data at the current node is represented by T, T_i is the subset obtained after splitting, and $sd(\cdot)$ is the standard deviation of the target variable.

To reduce overfitting and enhance generalizability of the model, the M5P model applies a smoothing mechanism between leaf nodes and parent nodes in the tree structure. This mechanism reduces discontinuities local linear regression equations and increases prediction stability. The smoothing coefficient is defined in (3):

$$\hat{y}_{smooth} = \frac{n.\hat{y}_{leaf} + k.\hat{y}_{parent}}{n+k} \quad (3)$$

In Equation (3), n denotes the number of samples at the leaf node and k is an integer constant. $\hat{y}_{leaf}$ is the predicted value from the leaf node, while $\hat{y}_{parent}$ denotes the predicted value obtained from the parent node.

The performance of the M5P model primarily depends on two core factors: the smoothness and complexity of the tree structure. Manual parameter tuning or grid search is often computationally expensive. Therefore, it is difficult to apply to complex datasets with noisy in water-cooled chiller data. Thus, an algorithm optimization method is needed to automatically adjust the parameters appropriately for the mode.

2.2. NSGA-III with Local Search Optimization

A hybrid algorithm, previously unmentioned within the theoretical framework of NSGA-III, based on design reference points for multidimensional target spaces, ensures both rapid convergence and diversity of solutions. The algorithm leverages crossover and mutation operators to determine a set of best-allocated Pareto-optimal points [29], particularly in thermodynamic conflict scenarios [30]. To further enhance its exploitability, a Local Search (LS) mechanism is integrated to fine-tune Pareto front candidates, preventing premature convergence and ensuring global optimality [31]. The NSGA-III-LS workflow, in this study for hyperparameter tuning, as shown in Fig. 1.

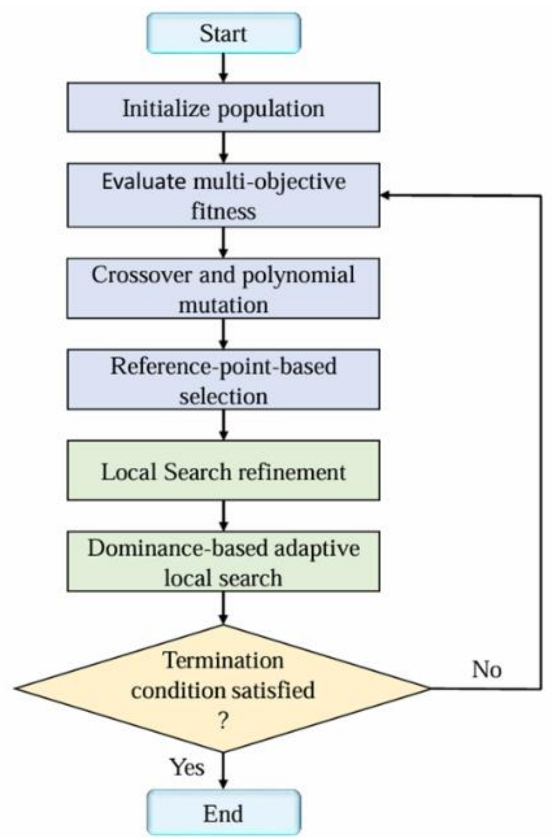

Figure 1. Flowchart of the proposed NSGA-III-LS optimization algorithm.

The dominance-based acceptance rule is used to ensure that the local search step does not degrade Pareto optimality or reduce population diversity.

In this work, the M5P calibration problem is treated as a D-dimensional many-objective optimization problem. Each individual in the population represents a candidate parameter vector, while multiple conflicting objectives are optimized simultaneously under bounded constraints. The individual solution x_i can be expressed as: $x_i = [x_{i,1}, x_{i,2}, \dots, x_{i,D}]$, $i = 1, 2, \dots, N_p$, where N_p denotes the population size and D is the number of decision variables. Each decision variable is subject to bound constraints: $x_j^{min} \le x_{i,j} \le x_j^{max}, j = 1, 2, \dots, D$. The many-objective optimization problem is expressed as:

$$\min_{x_i \in \Omega} f(x_i) = [f_1(x_i), f_2(x_i), \dots, f_M(x_i)] \quad (4)$$

2.2.1. Population initialization and evolutionary operators

The optimization process initializes an initial population $P^{(0)}$, randomly generated within a feasible search space defined by the lower and upper bounds of the decision variables.

$$x_{i,j}^{(0)} = x_j^{min} + rand(0,1)(x_j^{max} - x_j^{min}) \quad (5)$$

Then, based on NSGA-III genetic operators, both diversity and discovery in the decision space are supported. Simulated Binary Crossover (SBX) and polynomial mutation are applied in continuous optimization problems. Thanks to SBX, two parent individuals x_p and x_q are combined to create offspring that facilitate expanding the search space and improving the quality of solutions during iteration.

$$c_1, c_2 = SBX(x_p, x_q, p_c, \eta_c) \quad (6)$$

This process, p_c represents the probability of crossover, while $\eta_c$acts as a distribution index that adjusts the spread of offspring relative to parents. Polynomial mutation is then incorporated to maintain population diversity and minimize the risk of premature convergence.

After crossover and mutation, feasibility is strictly enforced by projecting each determinant variable onto its corresponding constraint bounds, $x_j^{min} \le x_{i,j} \le x_j^{max}, j = 1, 2, \dots, D$.

2.2.2. Reference-point-based selection

Once the parent and offspring populations are merged, NSGA-III performs environmental selection. All non-dominated fronts are preserved, whereas individuals in the last front are selected according to the perpendicular distance between the normalized objective vector f_i^{norm} and the corresponding reference point vector r_j. The normalization of objective vectors is shown in (7).

$$f_i^{norm} = \frac{f_i - f_{min}}{f_{max} - f_{min} + \epsilon}, \ m = 1,2, \dots, M \quad (7)$$

2.2.3. Local search enhancement

To improve convergence stability, the Local Search (LS) process is activated in the later stage of the evolutionary process. At this stage, several non-dominated solutions with good performance are selected based on their total normalized target value. These solutions are then locally fine-tuned by applying small random perturbations in the decision space. Accordingly, a candidate solution x_i' is generated from the current solution x_i, as defined in (8):

$$x_i' = x_i + stepSize(2 \cdot rand(1, D) - 1) \quad (8)$$

After candidate selection, a random vector $rand(1, D) \in [0,1]^D$ is generated and linearly transformed to $2 \cdot rand - 1$, resulting in symmetric perturbations within [-1,1]. This mechanism performs local search around the current solution, with a step that determines the radius of the search. All perturbations are strictly confined within the decision space. If the offspring x_i' dominate the original solution x_i, the current position will be updated $x_i \leftarrow x_i'$. After all generations are complete, the final Pareto front PF_{final} is obtained. Then, a multi-criteria decision process is performed to select a single compromise solution from the Pareto set; the compromise programming formulation is defined in (9) and (10):

$$f_i^{norm} \frac{f_i - f_{min}}{f_{max} - f_{min} + \epsilon}; \ i = 1, \dots, |PF_{final}| \quad (9)$$

The min-max normalization improves numerical stability. As a result, variables with larger numerical magnitudes are prevented from dominating the multi-objective optimization process. The target space is transformed into a normalized system. This maintains a uniform Pareto distribution and promotes an unbiased evolutionary search.

$$bestIdx = arg \min_i \sum_{m=1}^{M} f_{i,m}^{norm}, \ x_{best} = x_{bestIdx} \quad (10)$$

The final optimal vector x_{best} is extracted from the feasible region. Ensuring compliance with all operational constraints. The corresponding optimized hyperparameters are then used to train the M5P model, thereby determining the final architecture. This architecture is then used to implement the diagnostics.

2.3. Multi - Objective Strategy

The M5P model is primarily driven by two parameters, minLeaf and smoothK. The number of samples in each leaf affects how the tree grows. The smoothing coefficient then adjusts how the predictions are combined. Together, they affect the balance between complexity, generalizability, and stability [32]. When smoothK is set high, predictions tend to be smoother. With lower values, the model reacts more to local changes. In practice, different parameter settings can lead to quite different results. Therefore, these parameters often need to be systematically adjusted.

The problem in this study is formulated as a multi-objective optimization problem using the NSGA-III-LS algorithm, with a decision vector $x = [\text{minLeaf}, \text{smoothK}]$. The objective vector $F(x)$consists of criteria related to prediction accuracy and diagnostic performance, as defined in (11).

$$F(x) = [f_1(x), f_2(x), \dots, f_M(x)]^T \quad (11)$$

The objectives were considered based on predictive accuracy, correct/incorrect diagnostic ratios, and model performance. The optimization process on M5P is illustrated in Fig. 2. The residuals will be monitored by the EWMA chart. Details of the monitoring process will be presented later.

The dataset used in this study was obtained from the ASHRAE RP-1043 project, a well-known standard dataset in fault detection and diagnosis (FDD) [33]. The measured variables were collected from a real chiller operating under different load conditions. The reference model was established using only fault-free data. Only stable samples were retained by excluding outliers and transient fluctuations before model training. All input variables were min-max normalized to [0, 1] to improve numerical stability and optimization convergence. Two steady-state subsets containing 27 and 147 samples were merged to create a 174-sample training dataset for model calibration.

A total of 672 condenser fouling samples and 684 refrigerant leakage samples, covering four fault severity levels, were used to evaluate fault detection performance. These two faults are difficult to detect because of their slow progression and weak thermodynamic deviations. They mainly affect the condenser logarithmic mean temperature difference ($\mathrm{LMTD_{cd}}$) and the chiller performance index (ε_{sc}), which were selected due to their thermodynamic significance and sensitivity to system degradation.

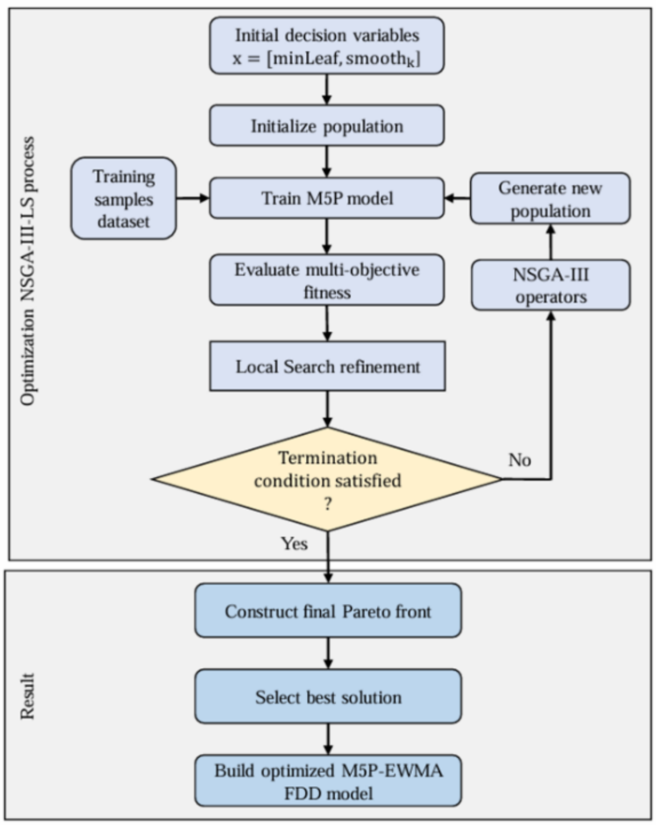

Figure 2. Parameter optimization flowchart of the M5P-EWMA model based on the NSGA-III-LS algorithm.

Although there are many variables in the ASHRAE RP-1043 dataset, only TCI, TCO, and Q_{ev} were selected because they best represent the thermodynamic behavior of refrigerant leakage and condenser fouling [34], [35]. Specifically, TCI and TCO reflect condenser heat transfer behavior, while Q_{ev} represents cooling capacity and system energy balance [36]. Using all available measurements may introduce redundancy and noise, whereas dimensionality reduction can improve model stability and feature separability [37], [38]. Therefore, feature selection should be based on physical relevance and fault sensitivity rather than using all available measurements, as this may introduce redundancy and additional noise without significantly improving fault separability [39].

Among the eight RP-1043 fault types, only condenser fouling and refrigerant leakage were chosen as sensitive diagnostic indicators of system degradation. These faults mainly affect $\mathrm{LMTD_{cd}}$ and ε_{sc}, which were selected as diagnostic indicators because of their thermodynamic sensitivity to system degradation. According to previous research reports, the detection rates are relatively low, ranging from 0-19.7% and 25-32% for condenser fouling and refrigerant leakage, and the misdiagnosis rate is approximately 4.1% at low severity levels (SL1-2) [40], [41]. The diagnostic rules and the corresponding impacts on characteristic parameters are summarized in Table 1, where "⬇" and "⬆" denote decreasing and increasing trends with increasing fault severity. During continuous activity, when scale buildup occurs in the condenser, it reduces heat transfer, leading to an increase in $\mathrm{LMTD_{cd}}$, while simultaneously reducing the heat exchange efficiency ε_{sc}. In addition, a refrigerant shortage reduces the condenser pressure and temperature, leading to a simultaneous decrease in both LMTD and ε. These thermodynamic relationships provide the physical basis for the proposed diagnostic approach.

Table 1. Description of characteristic behavior variables in a water-cooled chiller system.

Parameters	**Formulations**	**Fault type**	
		CdFoul	**RefLeak**
$\boldsymbol{\varepsilon_{sc}}$	$\varepsilon_{sc} = \dfrac{\mathrm{T_{sub}}}{\mathrm{T_{cd}} - \mathrm{TCI}}$	⬇	⬇
$\mathbf{LMTD_{cd}}$	$\mathrm{LMTD_{cd}} = \dfrac{\mathrm{TCO} - \mathrm{TCI}}{\frac{\mathrm{T_{cd}} - \mathrm{TCI}}{\mathrm{T_{cd}} - \mathrm{TCO}}}$	⬆	⬇

2.4. EWMA-Based Fault Detection Control Charts

An exponentially weighted moving average (EWMA) plot is used to improve sensitivity to small and slow deviations, enabling effective early fault detection [42]. The EWMA formulas for individual observations are given in (13) and (14).

$$\mathrm{EWMA_t} = Z_t = \lambda r_t + (1-\lambda) Z_{t-1} \tag{12}$$

In Equation (12), r_t represent the model residual at time t and λ $(0 < \lambda < 1)$ denotes the smoothing parameter with the initial condition $Z_1 = r_1$. To stay stable when processing high-frequency data, the M5P model employs a time-shifting smoothing mechanism. The tuning factor coefficient λ is chosen within the range of 0.05 to 0.25, balancing error sensitivity and arithmetic stability. This range also limits excessive smoothing, preventing the masking of early fault signals.

An EWMA chart with adaptive curved control limits (UCL/LCL) is employed to monitor the M5P model residuals, thereby enhancing sensitivity to small deviations compared with the conventional Shewhart chart.

$$\mathrm{UCL} = \mu_0 + L.\sigma\sqrt{\frac{\lambda}{2-\lambda}(1-(1-\lambda)^{2t}} \tag{13}$$

$$\mathrm{LCL} = \mu_0 - L.\sigma\sqrt{\frac{\lambda}{2-\lambda}(1-(1-\lambda)^{2t}} \tag{14}$$

In this model, L is set to 3 (99.73% confidence level), σ represents the residual standard deviation, and the residual mean is assumed to be zero. During the initial monitoring phase, these upper and lower limits are flexibly tightened, converging as the sample size increases to minimize false alarms while maintaining high detection sensitivity.

Fig. 3 below shows a two-stage model. In the offline stage, clean data are filtered. Outliers are removed, and steady-state patterns are retained. To improve model stability, statistical hyperparameters are derived from these residuals and then used to tune the EWMA control chart. During online operation, real-time data are compared with control limits. Values within indicate normal operation. Violations trigger fault detection and rule-based diagnosis.

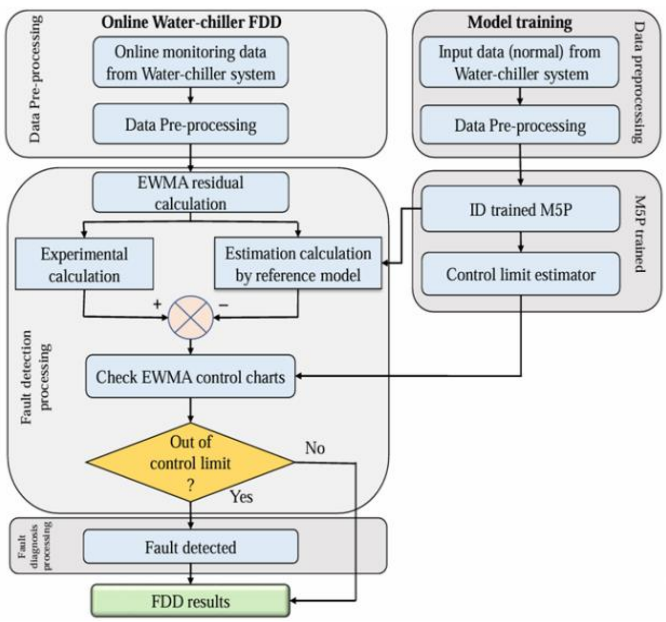

Figure 3. Workflow of the optimized M5P-based FDD framework.

The overall procedure of the proposed NSGA-III-LS-M5P-EWMA framework can be summarized as follows:

- Step 1: Acquire the raw ASHRAE RP-1043 experimental dataset reflecting various chiller operating conditions.
- Step 2: Preprocess the dataset through steady-state condition filtering, anomaly removal, thermodynamic feature selection, and normalization.
- Step 3: Initialize the NSGA-III-LS population for M5P hyperparameter optimization.
- Step 4: Perform crossover, mutation, non-dominated sorting, and reference-point-based environmental selection.
- Step 5: Apply the Local Search mechanism to refine elite Pareto solutions.
- Step 6: Select the optimal compromise solution and construct the optimized M5P model.
- Step 7: Generate prediction residuals between measured and predicted values.
- Step 8: Establish EWMA control limits under normal operating conditions.
- Step 9: Monitor online residual behavior and detect abnormal operating conditions.
- Step 10: Classify condenser fouling and refrigerant leakage severity levels based on the FDD indicators.

3. Experimental Setup

A single normal dataset is split 80/20 to train and test the M5P model. The test dataset is used to evaluate the predictive performance and stability of the model under normal operating conditions. Initial hyperparameter optimization was performed using the NSGA-III algorithm, with a population size Np = 60. The search was limited to two variables, minLeaf and smoothK, each within range [0, 100]. To deliver a high-performance FDD system, the simultaneous optimization process targeted three objectives: prediction accuracy, residual sensitivity, and false-positive minima. The optimization process aims to minimize RMSE and FAR while maximizing objective functions are normalized before being ranked based on the Pareto. This process was iterative over 50 generations, using a hybrid strategy and polynomial mutation to navigate the solution space. The crossover and mutation probabilities were set to 0.9 and 0.1, respectively [43]. The minLeaf parameter was rounded to the nearest integer after optimization for actual tree construction. NSGA-III uses an adaptive reference point strategy to maintain population diversity during evolution.

Upon completing the NSGA-III optimization phase, a local search (LS) strategy is implemented to enhance generalizability and prevent premature convergence. The elite 15% of non-dominated solutions undergo refinement using a predefined step size over 10 iterations. The convergence behavior of the normalized best objective values is shown Fig. 4. Optimized M5P hyperparameters are used to define baseline features. Residuals are then tracked with an EWMA chart for real-time fault detection. The last parameter represents the minimum samples per leaf. It is an integer, but treated as continuous during optimization to allow other searches. Consequently, the optimal value in Table 2 is presented in their fractional or scaled form, which are rounded to the nearest integer for actual model implementation and tree construction.

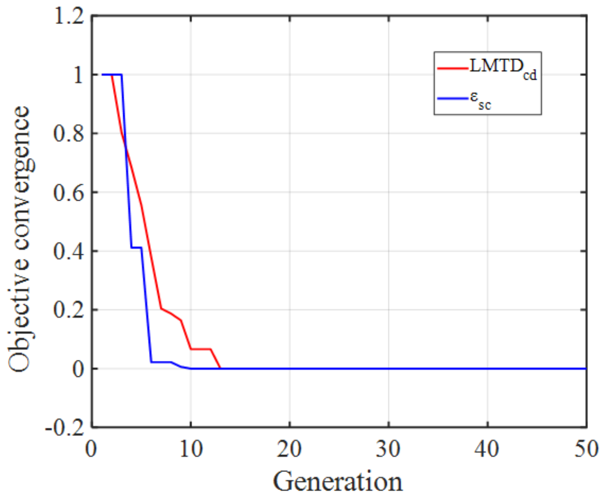

Figure 4. Convergence trend of the optimization process.

Table 2. Optimal M5P parameter values.

Parameters	**minLeaf**	**smoothK**
$\mathbf{LMTD_{cd}}$	0.0357	0.0508
$\boldsymbol{\varepsilon_{sc}}$	0.0357	0.0508

Prediction performance of the proposed method is evaluated using four statistical metrics: the coefficient of determination (R^2), root mean square error (RMSE), relative absolute error (RAE), and root standard error (RSE). While, R^2 measures the agreement between predicted and measured values. Prediction errors are quantified using RMSE, which is particularly sensitive to large deviations. In addition, RAE compares the model's performance to a mean-based reference, fitting HVAC data of varying magnitudes. The mathematical definitions of these metrics are given in (15)-(18).

$$R^2 = 1 - \frac{\sum_{i=1}^{n}(y_i - \hat{y}_i)^2}{\sum_{i=1}^{n}(y_i - \bar{y})^2} \tag{15}$$

$$\mathrm{RMSE} = \sqrt{\frac{1}{n}\sum_{i=1}^{n}(y_i - \hat{y}_i)^2} \tag{16}$$

$$\mathrm{RSE} = \sqrt{\frac{1}{n-D}\sum_{i=1}^{n}(y_i - \hat{y}_i)^2} \tag{17}$$

$$\mathrm{RAE} = \frac{\sum_{i=1}^{n}|y_i - \hat{y}_i|}{\sum_{i=1}^{n}|y_i - \bar{y}_i|} \tag{18}$$

The diagnostic performance is evaluated using three metrics: fault detection rate (FDR), false alarm rate (FAR), and missed detection rate (MDR). The FDR measures the proportion of fault samples that are correctly identified. By contrast, FAR represents the proportion of normal operating samples incorrectly identified as faults. MDR represents the proportion of fault samples incorrectly classified into other fault categories. The mathematical formulations of these metrics are given in (19)-(21).

$$\mathrm{FDR} = \frac{\mathrm{TP}}{\mathrm{TP+FN}} \tag{19}$$

$$\mathrm{FAR} = \frac{\mathrm{FP}}{\mathrm{FP+TN}} \tag{20}$$

$$\mathrm{MDR} = \frac{\mathrm{FN}}{\mathrm{TP+FN}} = 1 - \mathrm{FDR} \tag{21}$$

Fault detection and diagnosis of centrifugal chillers systems are performed using the NSGA-III-LS optimization strategy, M5P regression, and EWMA monitoring. NSGA-III-LS optimizes the M5P hyperparameters using a fault-free training dataset. The residuals between the calculated and predicted values obtained from the machine learning model are then used to determine performance thresholds for the two faults described in the dataset, as well as to evaluate standard FDD metrics.

4. Result and Discussion

For clarity, the key variables and performance indicators used in this study are defined as follows, since the faults mainly affect the condenser logarithmic mean temperature difference ($\mathrm{LMTD_{cd}}$) and the chiller performance index (ε_{sc}). The dataset used in this study from the benchmark ASHRAE RP-1043 project, which is widely adopted for chiller fault diagnosis research. The study focuses on the two most difficult-to-detect fault types, namely refrigerant leakage and condenser fouling. Other fault types were not considered because previous studies have reported detection and diagnosis rates close to 100%. The confidence level is 99.73%, corresponding (3σ).

4.1. Normal Operating Conditions

Three fault-free datasets, namely normal, normal-1, and the combined dataset, are used to evaluate the performance of the optimized NSGA-III-LS-M5P model. The main objective is to enhance fault detection at the fault onset stage, while balancing diagnostic accuracy and model stability.

The results from the graph in Fig. 5 demonstrate the superior performance of the NSGA-III-LS-M5P optimization method, achieving a prediction coefficient of determination (R^2) of 0.9967 for $\mathrm{LMTD_{cd}}$ and 0.9962 for ε_{sc}, significantly outperforming DE-LSSVR (R^2 of 0.9937 and 0.8697) and standard SVR (R^2 of 0.9868 and 0.8355). In particular, the proposed model reduces the prediction error of ε_{sc} to a very low level (0.0029), compared to 0.0281 for DE-LSSVR [40] and 0.0325 for SVR [41], representing an almost tenfold improvement in accuracy.

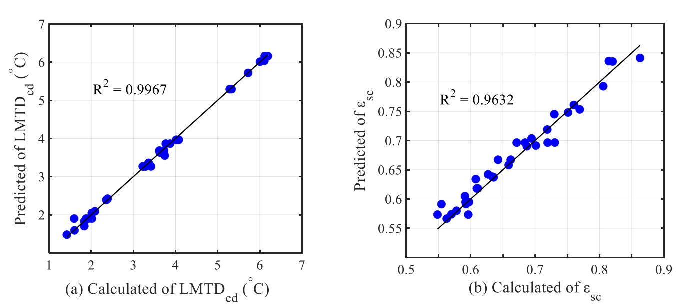

Figure 5. Predicted versus calculated values using normal data from ASHRAE RP-1043.

Physically, this high prediction accuracy of up to 99.67% ($\mathrm{LMTD_{cd}}$) and 99.32% (ε_{sc}) demonstrates that multi-objective balancing effectively achieves a balance between fault minimization and model generalization. Meanwhile, the data contain noise or outliers, SVR tends to fit these observations excessively, which may reduce its generalization capability and lead to overfitting [44]. Because, the NSGA-III-LS algorithm uses a reference-point mechanism to better characterize the nonlinear thermal dynamics and thermal inertia of the chiller. Noise filtering is improved while maintaining sensitivity to small oscillations, which enhances stability. As a result, the EWMA chart can effectively isolate energy losses.

Table 3 presents the results of the optimized model, which produces a significantly lower residual standard deviation. This results in tighter EWMA control limits, improving monitoring precision and stability. The 99.73% confidence level (3σ control limits) in EWMA-based monitoring is consistent with standard practice in fault detection studies, ensuring a balanced trade-off between false alarms and detection sensitivity. According to Table 4, the proposed framework achieves 100% classification accuracy with a false alarm rate of 0% for the “normal” and “normal-1” datasets at a 99.73% confidence interval. Although these results are comparable to those of the DE-LSSVR-EWMA method [40], they are significantly superior to the standard SVR-EWMA method [41]. Furthermore, these results show the proposed method's reliability and accuracy.

Table 3. Feature parameter results of SVR, DE-LSSVR, and NSGA-III-LS-M5P models on the RP-1043 dataset.

Models		Feature results	
		$LMTD_{cd}$	ε_{sc}
SVR	R^2	0.9868	0.8355
	σ_{SVR}	0.1517	0.0325
DE-LSSVR	R^2	0.9937	0.8697
	σ_{LSSVR}	0.1084	0.0281
NSGA-III-LS-M5P	R^2	0.9967	0.9632
	σ_{M5P}	0.0107	0.0029

Table 4. Diagnostic accuracy of FDD methods under normal conditions (99.73% confidence).

FDD methods	Normal		Normal-1	
	Correctly	Falsely	Correctly	Falsely
SVR-EWMA	86.20%	0%	76.20%	0%
DE-LSSVR-EWMA	100%	0%	100%	0%
NSGA-III-LS-M5P-EWMA	100%	0%	100%	0%

The radar charts (Fig. 6) describe the performance of the NSGA-III-LS-M5P model framework, with all evaluation metrics normalized to the range [0-1]. Normalization brings the accuracy and error metrics to the same scale, thereby providing an overview of the model’s performance. Detailed comparison of the results presented in Table 3 and Table 5 with those reported in previous studies further confirms the effectiveness of the proposed framework. Zhao et al. [41] reported that the SVR model achieved R^2 values of 0.9868 for $LMTD_{cd}$ and 0.8355 for ε_{sc}, while Tran et al. [40] improved the prediction performance using the DE-LSSVR model, achieving R^2 values of 0.9937 and 0.8697, respectively. In comparison, the proposed NSGA-III-LS-M5P framework achieved R^2 values of 0.9967 and 0.9632. The largest improvement was observed for ε_{sc}, where prediction errors were reduced by nearly an order of magnitude relative to SVR-based models.

Improvements achieved by DE-LSSVR suggest that parameter optimization has not yet been effective enough to fully describe complex nonlinear system characteristics. As noted by Li et al. (2020) and Ahmad et al. (2021), the predictive performance of LSSVR remains highly dependent on kernel selection and model parameterization [45], [46]. By contrast, M5P combines recursive partitioning with local linear regression, allowing different operating regimes to be modeled separately. This characteristic has been shown to improve prediction accuracy in complex energy and HVAC applications [18], which may further explain the great results achieved when the model is optimized using the NSGA-III-LS algorithm.

Focusing on the stability and reliability of the applied model, the prediction errors of the characteristic parameters under normal operating conditions are monitored using an EWMA control chart, which allows tracking the error dynamics over time. Fig. 7, shows that the prediction errors are tightly controlled within the EWMA control limits and exhibit stable behavior over time, with the $LMTD_{cd}$ error ranging from -0.033 (LCL); 0.0306 (UCL) and the ε_{sc} error ranging from -0.0078 (LCL); 0.0097 (UCL). Importantly, the absence of drift or accumulation near the control limits indicates low error and no model degradation. Moreover, the error distribution is close to a Gaussian distribution and centered around zero, demonstrating that the optimized M5P successfully captured the system's complex nonlinear relationships as shown in Table 6.

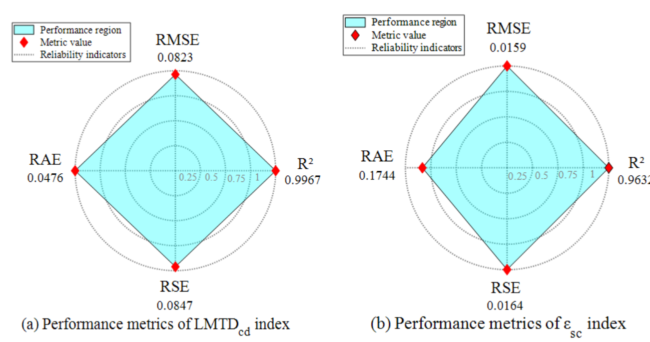

Figure 6. Performance evaluation of the NSGA-III-LS optimized M5P model for (a) $LMTD_{cd}$ and (b) ε_{sc}.

4.2. Fault Detection and Diagnosis Performance Evaluation

The fault detection and diagnosis results obtained using three different methods for two fault types under four severity levels are presented in Table 7.

4.2.1. Condenser heat exchanger fouling

The Fault Severity Index (FSI) classifies system conditions into four severity levels: Normal, Mild, Moderate and Severe based on predefined thresholds reflecting increasing deviations from normal operation.

Observing the graph in the initial phase, the system operates under normal conditions, with the FSI index remaining in the "Normal" region for both $LMTD_{cd}$ (Fig. 8(a), t < 500) and ε_{sc} in (Fig. 8(b), t < 300), confirming the stability of the method in suppressing operational noise. When the chiller system continues to operate, the FSI gradually exceeds 0.3, accurately reflecting the development of condenser fouling from mild to moderate levels. When the FSI approaches the maximum threshold (1), corresponding to the "Severe" region, the proposed NSGA-III-LS-M5P strategy effectively detects and accurately characterizes severe fouling.

Table 5. Performance of the reference model after optimization.

Method	Parameters	R^2	RMSE	RSE	RAE
NSGA-III-LS-M5P	$LMTD_{cd}$ ε_{sc}	0.9967 0.9632	0.0823 0.0159	0.0847 0.0164	0.0476 0.1744

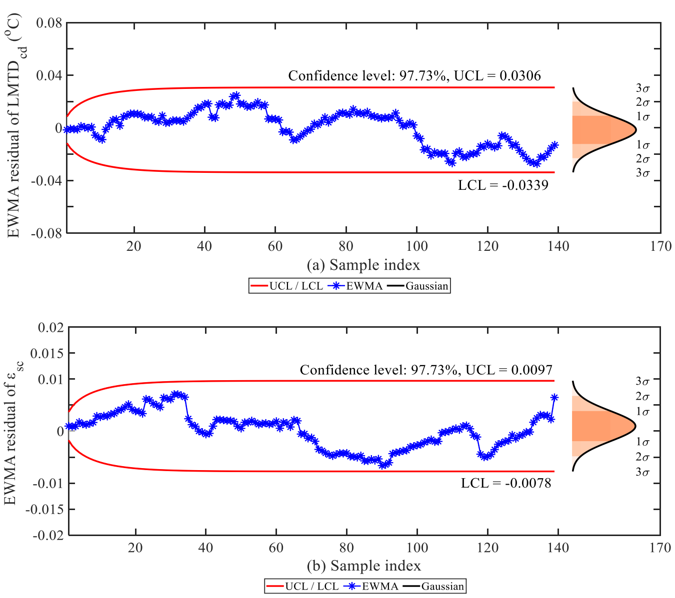

Figure 7. EWMA control charts used for monitoring residuals of (a) $LMTD_{cd}$ and (b) ε_{sc}.

Table 6. The control limits of $LMTD_{cd}$ and ε_{sc} for SVR, DE-LSSVR and NSGA-III-LS-M5P model applied to ASHRAE RP - 1043 dataset.

Methods	$LMTD_{cd}$		ε_{sc}	
	UCL	LCL	UCL	LCL
SVR-EWMA	0.1288	-0.1288	0.0285	-0.0285
DE-LSSVR-EWMA	0.0463	-0.0463	0.0103	-0.01203
NSGA-III-LS-M5P-EWMA	0.0306	-0.0339	0.0097	-0.0078

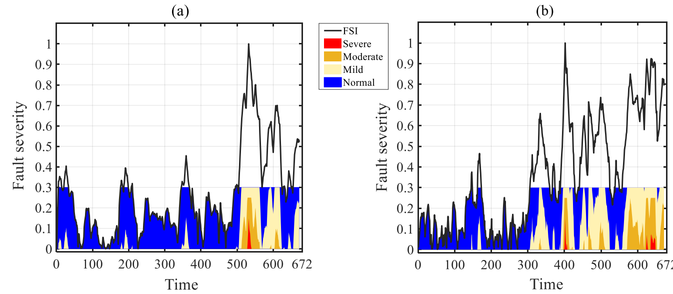

Figure 8. Time evolution of the fault severity index for real-time classification of condenser fouling severity: (a) $LMTD_{cd}$ and (b) ε_{sc}.

From a physical perspective, fouling increases thermal resistance and reduces the overall heat transfer coefficient, leading to a decrease in cooling effectiveness ε_{sc}. Therefore, the system compensates by increasing the temperature driving force, resulting in higher $LMTD_{cd}$ values. The combination of these factors explains the high FSI values observed.

The bar chart shows the performance of the proposed method for early fault detection and diagnosis. For the ε_{sc} signal, the proposed method achieves detection rates of 62.5%, 63.69%, 100%, and 100% at severity levels SL1-SL4. For $LMTD_{cd}$, the performance is even better, reaching 72.62% (SL1), 95.83% (SL2), 95.24% (SL3), and 100% (SL4), as shown in Fig. 9. The variation in early-stage detection performance is mainly due to the gradual development of condenser fouling and the distinct sensitivity of ε_{sc} and $LMTD_{cd}$ to early thermal performance degradation.

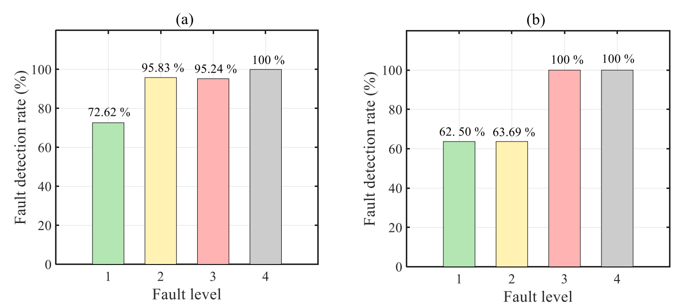

Figure 9. Fault detection rate as a function of condenser fouling severity for (a) $LMTD_{cd}$ and (b) ε_{sc}.

A comparison with previous studies reveals a significant improvement in early-stage fault diagnosis. Using the same dataset, Tran et al. [35] reported detection rates of only 0% and 19.7% for condenser fouling at SL1 and SL2, respectively, while Tran et al. [40] achieved 16.7% and 29.17% under the same operating conditions. In contrast, the proposed framework increased the detection rate to 62.5-72.62% at SL1 and over 95% at SL2. This substantial improvement exposes the limitations of previous methods in detecting incipient condenser fouling.

These findings demonstrate a clear advantage of the proposed framework over existing methods. RBF-EWMA [35], SVR-EWMA [41], and DE-LSSVR-EWMA [40] achieved relatively low detection rates at low fault severity levels and produced false alarm rates ranging from 3.8% to 10.7%. These results suggest that parameter optimization alone is insufficient for reliable incipient fault detection. In contrast, the NSGA-III-LS-M5P-EWMA consistently achieved higher detection rates with a minimized false alarm rate, particularly under low-severity fouling conditions where fault signatures are masked by operational variability. The combination of M5P and dual optimization improves fault separability, enabling earlier and more reliable detection.

4.2.2. Refrigerant leakage

The graph in Fig. 10 shows that both indicators are in the "Normal" region (FSI < 0.2) until approximately t ≈ 300, confirming no false alarms. When refrigerant leakage occurs, $LMTD_{cd}$ signal responds earlier, with the FSI increasing to about 0.3-0.6 during t ≈ 350-450, due to its high sensitivity to initial performance degradation. The loss of refrigerant reduces mass flow rate and the liquid level in the condenser, weakening the cooling process below the boiling point and causing an immediate decrease in cooling efficiency.

Meanwhile, the ε_{sc} signal responds more slowly but more strongly, with FSI increasing clearly only after t > 500. A clear delay is observed. The system tries to compensate for the reduced heat transfer by increasing the condensing temperature, which leads to a larger temperature difference. Higher deviations are observed. When the refrigerant leakage becomes severe, both indicators move into the "Severe" region (FSI ≈ 1). Strong degradation occurs, and the thermodynamic cycle is clearly disrupted. The results show that the proposed framework can capture the physical degradation caused by refrigerant mass loss.

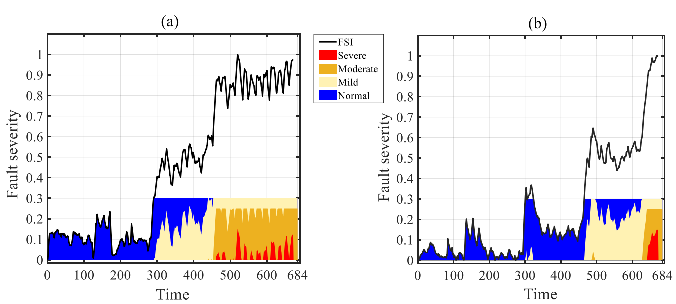

Figure 10. Time evolution of the fault severity index for real-time classification of refrigerant leakage severity: (a) $LMTD_{cd}$ and (b) ε_{sc}.

To evaluate sensitivity at different fault levels, the detection performance for refrigerant leakage is shown in Fig. 11(a) and Fig. 11(b). Based on the ε_{sc} index, the proposed method achieves FDR values of 87.50%, 76.79%, 100%, and 100% for SL1 to SL4, while maintaining the false alarm rate at 0%. The small difference between SL1 and SL2 is attributed to the slow progression of refrigerant leakage, which only causes minor thermodynamic disturbances and keeps the ε_{sc} variations close to normal operating fluctuations. Therefore, refrigerant leak detection is still a big problem for a lot of current FDD methods. In the study by Zhao et al. [41], detection rates of only 20.1% and 36.2% were reported for SL1 and SL2, respectively, with false alarm rates of 7.1% using the SVR-EWMA method.

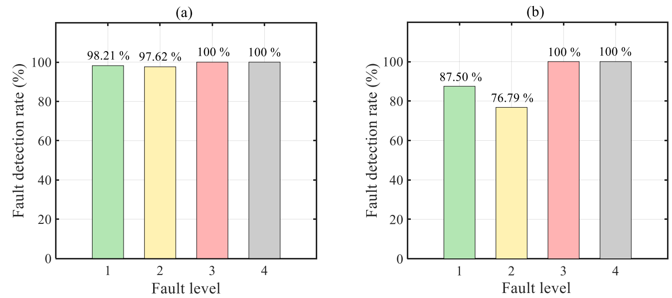

Figure 11. Fault detection rate as a function of refrigerant leakage severity for (a) $LMTD_{cd}$ and (b) ε_{sc}.

Although Tran et al. (2016) [40], achieved modest improvements of 37.43% and 39.77% through DE-based optimization, the false alarm rate still reached 9.9% at the SL1 fault severity level. The DE-LSSVR method is parameter-optimized and achieved 100% detection at higher fault severity levels (SL3-SL4), but its performance under incipient fault conditions remained insufficiently reliable for accurate fault identification.

Table 7 shows that parameter optimization alone is insufficient to ensure reliable initial fault detection. Although the DE-LSSVR method achieved a 100% detection rate at SL3-SL4, its performance deteriorated under mild leakage conditions because weak fault signatures were still difficult to distinguish from normal operating variations. This suggests that improving initial fault detection depends not only on parameter optimization but also on a suitable model structure.

An overview of the results shows that the proposed NSGA-III-LS hybrid optimization strategy improves convergence speed while maintaining the interpretability and adaptability of the M5P model for multi-objective optimization. Compared to GA, PSO, Grid Search, and Bayesian optimization for general hyperparameter tuning, NSGA-III-LS offers a better balance between prediction accuracy, stability, and false alarm rate [22], [23]. In addition, NSGA-III enhances diversity preservation and robustness in Pareto-based search [26]. Although its application in chiller fault diagnosis remains limited, this provides further impetus for its use in the current study.

Thanks to its transparent model structure, the proposed method allows more effective capture of nonlinear thermodynamic relationships compared to methods such as [44]. Tables and figures show that this method achieves high diagnostic accuracy for early fault detection, along with good model stability and a low false alarm rate. The proposed method shows its feasibility in handling the complex behavior of water chillers and supporting reliable system operation.

Notably, this research framework proves efficacious even with limited data, a common challenge in HVAC applications. It also has the ability to identify incipient faults, particularly condenser fouling and refrigerant leakage, faults that are difficult to distinguish in the early stages of development. This capability supports proactive maintenance and can contribute to energy savings of 15-30% [1], [5]. Although the proposed framework performs well on the ASHRAE RP-1043 dataset, its effectiveness under real-world operating conditions, such as sensor noise, missing data, seasonal variations, and dynamic load changes, still requires further evaluation.

Ultimately, the proposed framework gives a useful basis for improving the operational reliability of real-world systems. With appropriate adaptation, it can be applied to more complex industrial environments and extended to diagnose a wider variety of faults.

Table 7. Detection performance of three models at different fault severity levels.

Parameter	FDD strategy	Severity level 1 (C/F)	Severity level 2 (C/F)	Severity level 3 (C/F)	Severity level 4 (C/F)
	Condenser fouling				
ε_{sc}	SVR-EWMA	0.0/0.0	19.7/0.0	65.5/4.4	100/0.0
	DE-LSSVR-EWMA	16.7/6.5	29.17/0.0	76.79/10.7	100/0.0
	Proposed	87.5/0.0	76.79/0.0	100/0.0	100/0.0
	Refrigerant leakage				
ε_{sc}	SVR-EWMA	20.1/2.6	36.2/7.1	88.3/1.1	100/0.0
	DE-LSSVR-EWMA	37.43/9.9	39.77/0.0	100/0.0	100/0.0
	Proposed	62.5/0.0	63.69/0.0	100/0.0	100/0.0

C/F = Correctly diagnosed/ Falsely diagnosed (%)

5. Conclusion

Based on the ASHRAE RP-1043 dataset, the proposed framework shows good performance in fault detection and diagnosis under limited-data conditions. The combination of the NSGA-III-LS multi-objective optimization algorithm and the M5P model improves the predictive performance of the diagnostic framework for nonlinear and noisy water-cooled chiller systems. Moreover, the integration of a two-stage optimization strategy with EWMA monitoring increases fault detection sensitivity while reducing false alarms, making early fault detection more effective.

This research integrated machine learning modeling, multi-objective optimization, and statistical process monitoring into a fault detection and diagnosis framework for centrifugal water chillers. The developed approach improved diagnostic accuracy by 30-50%, particularly for incipient faults. It also supported predictive maintenance planning, enhanced system reliability, and promoted energy efficiency.

Strong potential is shown for improving FDD performance in HVAC systems. However, the study is limited to a benchmark dataset and a restricted set of fault types. Further validation using field data and a wider range of fault scenarios is required to assess its applicability to different chiller systems and operating environments.

Acknowledgements

The authors gratefully acknowledge the support and technical assistance provided by the Faculty of Heat and Refrigeration Engineering, Industrial University of Ho Chi Minh City, Viet Nam.

Conflict of interest

The authors declare that there are no conflicts of interest regarding the publication of this manuscript.

Nomenclature

LCL	lower control limit
UCL	upper control limit
L	width of the control limit
TEO	evaporator outlet water temperature [º C]
TCI	condenser inlet water temperature [º C]
Q	chiller cooling load [kW]
SL	severity level

Symbols

ϵ	residual (error) term
σ	standard deviation of residuals
λ	tunning factor
μ	mean value

Subscripts

cd	condenser
sc	sub-cooling
t	time

Author Contribution Statement

Nguyen Duc Thanh proposed the research problem, developed the theoretical framework, performed the computational analysis, and wrote the manuscript.

Dinh Anh Tuan Tran reviewed, evaluated, edited, and contributed to the presentation of the research results.

Data Availability

Data for this study were obtained from the ASHRAE RP-1043 project. The dataset is subject to licensing restrictions and cannot be publicly released. Access may be provided by the corresponding author with ASHRAE approval upon reasonable request.

References

[1] P. M. Cuce and E. Cuce, “Role of HVAC in Building Energy Consumption: A Critical Review,” Journal of Thermal Analysis and Calorimetry, vol. 151, pp. 3059–3080, Feb. 2026. doi: https://doi.org/10.1007/s10973-026-15322-9.

[2] Z. Wang *et al.*, "Examining the impact of common faults on chiller performance through experimental investigation and parameter sensitivity analysis", *Energy Build.*, vol. 317, p. 114389, Aug. 2024, doi: https://doi.org/10.1016/j.enbuild.2024.114389.

[3] Z. Wang, J. Guo, S. Zhou, and P. Xia, "Performance Evaluation of Chiller Fault Detection and Diagnosis Using Only Field-Installed Sensors", *Processes*, vol. 11, no. 12, p. 3299, Nov. 2023, doi: https://doi.org/10.3390/pr11123299.

[4] A. Gharbi, M. Ayari, N. Albalawi, Y. E. Touati, and Z. Klai, "Intelligent HVAC Control: Comparative Simulation of Reinforcement Learning and PID Strategies for Energy Efficiency and Comfort Optimization", *Mathematics*, vol. 13, no. 14, p. 2311, Jul. 2025, doi: https://doi.org/10.3390/math13142311.

[5] J. Bi *et al.*, "AI in HVAC fault detection and diagnosis: A systematic review", *Energy Rev.*, vol. 3, no. 2, p. 100071, Jun. 2024, doi: https://doi.org/10.1016/j.enrev.2024.100071.

[6] A. Rafati, H. R. Shaker, and S. Ghahghahzadeh, "Fault Detection and Efficiency Assessment for HVAC Systems Using Non-Intrusive Load Monitoring: A Review", *Energies*, vol. 15, no. 1, p. 341, Jan. 2022, doi: https://doi.org/10.3390/en15010341.

[7] I. Matetić, I. Štajduhar, I. Wolf, and S. Ljubic, "A Review of Data-Driven Approaches and Techniques for Fault Detection and Diagnosis in HVAC Systems", *Sensors*, vol. 23, no. 1, p. 1, Dec. 2022, doi: https://doi.org/10.3390/s23010001.

[8] H. Wang, D. Mai, Q. Li, and Z. Ding, "Evaluating Machine Learning Models for HVAC Demand Response: The Impact of Prediction Accuracy on Model Predictive Control Performance", *Buildings*, vol. 14, no. 7, p. 2212, Jul. 2024, doi: https://doi.org/10.3390/buildings14072212

[9] Z. Soltani, K. K. Sørensen, J. Leth, and J. D. Bendtsen, "Fault detection and diagnosis in refrigeration systems using machine learning algorithms", *Int. J. Refrig.*, vol. 144, pp. 34–45, Dec. 2022, doi: https://doi.org/10.1016/j.ijrefrig.2022.08.008.

[10] P. Movahed, S. Taheri, and A. Razban, "A bi-level data-driven framework for fault-detection and diagnosis of HVAC systems", *Appl. Energy*, vol. 339, p. 120948, Jun. 2023, doi: https://doi.org/10.1016/j.apenergy.2023.120948.

[11] I. D. L. Á. Fallas Calderón, M. K. Heenkenda, T. S. Sahota, and L. S. Serrano, "Canola Yield Estimation Using Remotely Sensed Images and M5P Model Tree Algorithm", *Remote Sens.*, vol. 17, no. 13, p. 2127, Jun. 2025, doi: https://doi.org/10.3390/rs17132127.

[12] A. Behnood and D. Daneshvar, "A machine learning study of the dynamic modulus of asphalt concretes: An application of M5P model tree algorithm", *Constr. Build. Mater.*, vol. 262, p. 120544, Nov. 2020, doi: https://doi.org/10.1016/j.conbuildmat.2020.120544

[13] H. U. Ahmed, A. S. Mohammed, and A. A. Mohammed, "Proposing several model techniques including ANN and M5P-tree to predict the compressive strength of geopolymer concretes incorporated with nano-silica", *Environ. Sci. Pollut. Res.*, vol. 29, no. 47, pp. 71232–71256, Oct. 2022, doi: https://doi.org/10.1007/s11356-022-20863-1.

[14] P. Jimeno-Sáez, R. Martínez-España, J. Casalí, J. Pérez-Sánchez, and J. Senent-Aparicio, "A comparison of performance of SWAT and machine learning models for predicting sediment load in a forested Basin, Northern Spain", *CATENA*, vol. 212, p. 105953, May 2022, doi: https://doi.org/10.1016/j.catena.2021.105953.

[15] F. Hutter, L. Kotthoff, and J. Vanschoren, *Automated Machine Learning.* Cham: Springer International Publishing, 2019. doi: https://doi.org/10.1007/978-3-030-05318-5.

[16] M. Kaveh and M. S. Mesgari, "Application of Meta-Heuristic Algorithms for Training Neural Networks and Deep Learning Architectures: A Comprehensive Review", *Neural Process. Lett.*, vol. 55, no. 4, pp. 4519–4622, Aug. 2023, doi: https://doi.org/10.1007/s11063-022-11055-6.

[17] A. Gogna and A. Tayal, "Metaheuristics: review and application", *J. Exp. Theor. Artif. Intell.*, vol. 25, no. 4, pp. 503–526, Dec. 2013, doi: https://doi.org/10.1080/0952813X.2013.782347.

[18] A. K. Srivastava *et al.*, "A Day-Ahead Short-Term Load Forecasting Using M5P Machine Learning Algorithm along with Elitist Genetic Algorithm (EGA) and Random Forest-Based Hybrid Feature Selection", *Energies*, vol. 16, no. 2, p. 867, Jan. 2023, doi: https://doi.org/10.3390/en16020867.

[19] Y. Xia, J. Zhao, Q. Ding, and A. Jiang, "Incipient Chiller Fault Diagnosis Using an Optimized Least Squares Support Vector Machine with Gravitational Search Algorithm", *Front. Energy Res.*, vol. 9, p. 755649, Nov. 2021, doi: https://doi.org/10.3389/fenrg.2021.755649.

[20] Y. Liu, T. Liang, M. Zhang, N. Jing, Y. Xia, and Q. Ding, "Fault Diagnosis of Centrifugal Chiller Based on Extreme Gradient Boosting", *Buildings*, vol. 14, no. 6, p. 1835, Jun. 2024, doi: https://doi.org/10.3390/buildings14061835.

[21] M. Li, H. Tao, M. Liu, and T. He, "Study on enhanced fault diagnosis of chiller units in HVAC systems under the imbalanced data environment using GA-Optimized LightGBM", *Energy Build.*, vol. 330, p. 115360, 2025. doi: https://doi.org/10.1016/j.enbuild.2025.115360

[22] T. Ghosh and K. Martinsen, "Generalized approach for multi-response machining process optimization using machine learning and evolutionary algorithms", *Eng. Sci. Technol. Int. J.*, vol. 23, no. 3, pp. 650–663, Jun. 2020, doi: https://doi.org/10.1016/j.jestch.2019.09.003.

[23] F. Mostafazadeh, S. J. Eirdmousa, and M. Tavakolan, "Energy, economic and comfort optimization of building retrofits considering climate change: A simulation-based NSGA-III approach", *Energy Build.*, vol. 280, p. 112721, Feb. 2023, doi: https://doi.org/10.1016/j.enbuild.2022.112721.

[24] L. Gao, D. Li, and N. Liang, "Genetic algorithm-aided ensemble model for sensor fault detection and diagnosis of air-cooled chiller system", *Build. Environ.*, vol. 233, p. 110089, Apr. 2023, doi: https://doi.org/10.1016/j.buildenv.2023.110089.

[25] L. Ma and D. Zou, "An Improved NSGA-III With Hybrid Crossover Operator for Multi-Objective Optimization of Complex Combined Cooling, Heating, and Power Systems", *Energy Sci. Eng.*, vol. 13, no. 4, pp. 1509–1543, Apr. 2025, doi: https://doi.org/10.1002/ese3.2039.

[26] K. Deb and H. Jain, "An Evolutionary Many-Objective Optimization Algorithm Using Reference-Point-Based Nondominated Sorting Approach, Part I: Solving Problems with Box Constraints", *IEEE Trans. Evol. Comput.*, vol. 18, no. 4, pp. 577–601, Aug. 2014, doi: https://doi.org/10.1109/TEVC.2013.2281535.

[27] J. R. Quinlan, "Combining instance-based and model-based learning", presented at the Proceedings of the tenth international conference on machine learning, 1993, pp. 236–243. https://dl.acm.org/doi/10.5555/3091529.3091560

[28] Y. Wang and I. H. Witten, "Inducing model trees for continuous classes", presented at the Proceedings of the ninth European conference on machine learning, vol. 9, no.1, pp. 128–137. 1997. Wang-Witten-Induct.pdf

[29] Q. Gu, Q. Xu, and X. Li, "An improved NSGA-III algorithm based on distance dominance relation for many-objective optimization", *Expert Syst. Appl.*, vol. 207, p. 117738, Nov. 2022, doi: https://doi.org/10.1016/j.eswa.2022.117738.

[30] Z.-M. Gu and G.-G. Wang, "Improving NSGA-III algorithms with information feedback models for large-scale many-objective optimization", *Future Gener. Comput. Syst.*, vol. 107, pp. 49–69, Jun. 2020, doi: https://doi.org/10.1016/j.future.2020.01.048.

[31] M. Hazbei, N. Rafati, N. Kharma, and U. Eicker, "Optimizing architectural multi-dimensional forms; a hybrid approach integrating approximate evolutionary search, clustering and local optimization", *Energy Build.*, vol. 318, p. 114460, Sep. 2024, doi: https://doi.org/10.1016/j.enbuild.2024.114460.

[32] P. Sihag, S. Mohsenzadeh Karimi, and A. Angelaki, "Random Forest, M5P and regression analysis to estimate the field unsaturated hydraulic

conductivity", *Appl. Water Sci.*, vol. 9, no. 5, p. 129, Jul. 2019, doi: https://doi.org/10.1007/s13201-019-1007-8.

[33] M. C. Comstock, J. E. Braun, and R. Bernhard, *Development of analysis tools for the evaluation of fault detection and diagnostics in chillers*. Master Thesis, 45870. Purdue University,ME, DEC, 1999. https://purdue.primo.exlibrisgroup.com/discovery/fulldisplay/alma99130475630001081/01PURDUE_PUWL:PURDUE

[34] Q. Zhou, S. Wang, and F. Xiao, "A Novel Strategy for the Fault Detection and Diagnosis of Centrifugal Chiller Systems", *HVACR Res.*, vol. 15, no. 1, pp. 57–75, Jan. 2009, doi: https://doi.org/10.1080/10789669.2009.10390825.

[35] D. A. T. Tran, Y. Chen, M. Q. Chau, and B. Ning, "A robust online fault detection and diagnosis strategy of centrifugal chiller systems for building energy efficiency", *Energy Build.*, vol. 108, pp. 441–453, Dec. 2015, doi: https://doi.org/10.1016/j.enbuild.2015.09.044.

[36] X. Zhao, M. Yang, and H. Li, "A virtual condenser fouling sensor for chillers", *Energy Build.*, vol. 52, pp. 68–76, Sep. 2012, doi: https://doi.org/10.1016/j.enbuild.2012.05.018.

[37] V. Bolón-Canedo and B. Remeseiro, "Feature selection in image analysis: a survey", *Artif. Intell. Rev.*, vol. 53, no. 4, pp. 2905–2931, Apr. 2020, doi: https://doi.org/10.1007/s10462-019-09750-3.

[38] H. Kabir and N. Garg, "Machine learning enabled orthogonal camera goniometry for accurate and robust contact angle measurements", *Sci. Rep.*, vol. 13, no. 1, p. 1497, Jan. 2023, doi: https://doi.org/10.1038/s41598-023-28763-1.

[39] Y. Bezyan, F. Nasiri, and M. Nik-Bakht, "Feature Selection and Fault Detection Under Dynamic Conditions of Chiller Systems", *Electronics*, vol. 15, no. 1, p. 208, Jan. 2026, doi: https://doi.org/10.3390/electronics15010208.

[40] D. A. T. Tran, Y. Chen, H. L. Ao, and H. N. T. Cam, "An enhanced chiller FDD strategy based on the combination of the LSSVR-DE model and EWMA control charts", *Int. J. Refrig.*, vol. 72, pp. 81–96, Dec. 2016, doi: https://doi.org/10.1016/j.ijrefrig.2016.07.024.

[41] Y. Zhao, S. Wang, and F. Xiao, "A statistical fault detection and diagnosis method for centrifugal chillers based on exponentially-weighted moving average control charts and support vector regression", *Appl. Therm. Eng.*, vol. 51, no. 1–2, pp. 560–572, Mar. 2013, doi: https://doi.org/10.1016/j.applthermaleng.2012.09.030

[42] J. Liu *et al.*, "A statistical-based online cross-system fault detection method for building chillers", *Build. Simul.*, vol. 15, no. 8, pp. 1527–1543, Aug. 2022, doi:https://doi.org/10.1007/s12273-021-0877-5

[43] A. Moayedikia, S. Fin, and U. K. Wiil, "Multi-objective optimization formulation for Alzheimer’s disease trial patient selection", *J. Biomed. Inform.*, vol. 172, p. 104955, Dec. 2025, doi: https://doi.org/10.1016/j.jbi.2025.104955.

[44] H.-L. Shieh and C.-C. Kuo, "A reduced data set method for support vector regression", *Expert Syst. Appl.*, vol. 37, no. 12, pp. 7781–7787, Dec. 2010, doi: https://doi.org/10.1016/j.eswa.2010.04.062.

[45] C. Li, Y. Shao, D. Zhao, Y. Guo, and X. Hua, "Feature selection for high-dimensional regression via sparse LSSVR based on Lp-norm", *Int. J. Intell. Syst.*, vol. 36, no. 2, pp. 1108–1130, Feb. 2021, doi: https://doi.org/10.1002/int.22334.

[46] M. F. Ahmad, N. A. M. Isa, W. H. Lim, and K. M. Ang, 'Differential evolution: A recent review based on state-of-the-art works", *Alex. Eng. J.*, vol. 61, no. 5, pp. 3831–3872, May 2022, doi: https://doi.org/10.1016/j.aej.2021.09.013.